Acta Cryst. (1999). A**55**, 719–728

A new type of constraint in the maximum-entropy method using ambiguous phase information from anomalous-scattering powder data

K. Burger* and W. Prandl

Institut für Kristallographie, Universität Tübingen, Charlottenstrasse 33, D-72070 Tübingen, Germany.
E-mail: karsten.burger@uni-tuebingen.de

(*Received 24 February 1998; accepted 2 January 1999*)

Abstract

Anomalous scattering of X-rays at a synchrotron source can be used for the *ab initio* structure determination of unknown crystal structures using only powder diffraction data. For noncentrosymmetric crystals, the phases of structure factors can only be determined with a remaining ambiguity, when one chemical element is used as resonant scatterer. A corresponding additional constraint function has been built into an enhanced version of the program *MEED*, so that now all types of information gained from an anomalous-scattering powder diffraction experiment can be used in a maximum-entropy calculation of the electron-density distribution: phased reflections, unphased reflections, intensities of groups of overlapping reflections, and now also reflections with a remaining ambiguity in the phase. This is important for practical use, since a lot of information is already lost in the powder diagram compared with single-crystal datasets and it is essential to use all remaining information. The new constraint is demonstrated with the structure of Cu_5Zn_8.

1. Introduction

1.1. *Anomalous scattering and powder data*

It is well known that anomalous scattering of X-rays from a synchrotron source can be used for the *ab initio* structure determination of unknown crystal structures using only powder diffraction data (Prandl, 1990, 1994; Limper *et al.*, 1991; Burger *et al.*, 1997; Burger, 1997; Burger *et al.*, 1998). We use the same notation as in Burger *et al.* (1997), shown in Table 1. Compared with the single-crystal MAD method (Hendrickson, 1991), the use of powder data is hindered by the non-avoidable overlap of the Friedel reflections **H** and $-\mathbf{H}$ in a single powder pattern line, and also due to other exact coincidences or severe overlap of symmetrically non-equivalent reflections.

Nevertheless, it has been shown that from at least two powder patterns (one with the wavelength near-edge and one far-edge of an absorption edge of a chemical element contained in the sample) difference and partial Patterson densities can be calculated that are much easier to interpret than the usual Patterson density. These can be used, for example, to locate the resonant scatterer atoms (r.s.), so that their substructure is solved. With this knowledge, their contribution $F_0^\sigma = |F_0^\sigma| \exp(i\Psi_\sigma)$ to the reflections may be calculated.

In a second step of the calculation, phases Φ of structure factors $F = |F| \exp(i\Phi) = A + iB$ can be calculated for the unique reflections in the powder pattern, but not for reflections overlapping with other non-equivalent reflections in one powder line. The basis for the calculations is equation (1): from the integrated powder-line intensity, only the average intensity $\bar{I}(\lambda)$ of the Friedel pair can be determined,

$$\begin{aligned}\bar{I}(\lambda) &\equiv \tfrac{1}{2}\left[|F(\mathbf{H})|^2 + |F(-\mathbf{H})|^2\right] \\ &= |F_0|^2 + 2e_\sigma(\lambda)|F_0^\sigma||F_0| \cos(\Phi - \Psi_\sigma) \\ &\quad + |a_\sigma(\lambda)|^2 |F_0^\sigma|^2. \end{aligned} \tag{1}$$

In the case of a centrosymmetric crystal, and if the origin of the unit cell is chosen to coincide with the center of inversion (which is always possible), only signs have to be determined, $\cos\Phi = \pm 1$, $\cos\Psi_\sigma = \pm 1$, and two measurements of $\bar{I}(\lambda)$ near- and far-edge are sufficient to obtain the phase Φ. In the noncentrosymmetric case, however, a single r.s. type with its absorption edge is not sufficient to determine the phase uniquely, since only the information $\cos(\Phi - \Psi_\sigma) = \cos\Delta$ is obtained (Ψ_σ is supposed to be known at this stage), and with it the information on $|\sin\Delta| = (1 - \cos^2\Delta)^{1/2}$, but not the information on the sign of the sine term, $\sin\Delta = \pm|\sin\Delta|$. In this way, there remains an ambiguity in the phase determination for noncentrosymmetric crystals.

Prandl (1990) suggested the use of a second type of r.s. to overcome this ambiguity, but this seems to be difficult for practical reasons. Thus, phase determination from powder data is severely hindered and a Fourier calculation of the electron density is not possible, since only half of the phase information is available even for the unique reflections in the powder diagram, and no phase information for the non-unique ones or the reflections, where the r.s. atoms do not contribute significantly, $|F_0^\sigma| \ll |F_0|$. A solution of this problem is

Table 1. *List of symbols used in the text*

r.s.	Resonantly scattering atom
f, f', f''	Atomic form factor and resonance corrections including an isotropic temperature factor
$f_\sigma = f_{0\sigma} + f'_\sigma + if''_\sigma$	Form factor for the r.s.
$F_0(\mathbf{H}) \equiv F_0 \equiv \lvert F_0\rvert \exp(i\Phi)$	Total structure factor of reflection **H** under consideration, without resonance contributions
$F_0^\sigma(\mathbf{H}) \equiv F_0^\sigma \equiv \lvert F_0^\sigma\rvert \exp(i\Psi_\sigma)$	Structure factor of the r.s. alone
$\overline{I}(\lambda) \equiv [\lvert F(\mathbf{H})\rvert^2 + \lvert F(-\mathbf{H})\rvert^2]/2$	Mean intensity of a Friedel pair of reflections **H** and $-\mathbf{H}$
$a_\sigma(\lambda) \equiv (f'_\sigma + if''_\sigma)/f_{0\sigma}$	Resonance contributions to the form factor in units of f_0^σ.
$e_\sigma(\lambda) \equiv f'_\sigma/f_{0\sigma}$	
I_i, $f_{\sigma i}$, e_i and a_i^2	Shorthand symbols for $\overline{I}(\lambda_i)$, $f_\sigma(\lambda_i)$, $e_\sigma(\lambda_i)$ and $\lvert a_\sigma(\lambda_i)\rvert^2$, respectively.

now presented using a new constraint type in the maximum-entropy algorithm.

1.2. *Maximum-entropy method (MEM)*

The nonlinear MEM, which has its roots in probability and information theory, has been applied to many fields of crystallography (for a current review, see Gilmore, 1996). This includes: an attempt to see non-nuclear density maxima with precise silicon data directly (Sakata & Sato, 1990; Takata & Sakata, 1996); application to powder data sets with overlapping reflections (Sakata *et al.*, 1990); application to neutron data, where negative scattering densities can occur (Takata *et al.*, 1994); disordered structures (Papoular *et al.*, 1992); polarized neutron scattering (Papoular *et al.*, 1995; Schleger *et al.*, 1997); extraction of strictly positive integrated intensities from strongly overlapping powder reflections (Sivia & David, 1994); quasicrystals (Haibach & Steurer, 1996); single-crystal Laue data sets (Bourenkov *et al.*, 1996); phase determination by statistical (direct) methods (Bricogne & Gilmore, 1990).

Although the current MEM algorithms are far from being perfect [see *e.g.* Iversen *et al.* (1997) and references therein], it has been shown to be very well suited for the calculation of electron densities using incomplete powder data sets as described above, since it can use all the different information obtained in one calculation (Burger *et al.*, 1997; Burger, 1997).

From the anomalous-scattering data sets, four sets of reflections are obtained, which can now all be used in the MEM calculation (listed in order of decreasing information content):

(i) one set of signed reflections (with F_0 known, '*F*-constraint');

(ii) a set of ambiguous phase information as described above, when the crystal is noncentrosymmetric and $\cos\Delta$ is known, but only $\lvert\sin\Delta\rvert$ without its correct sign (the new '*A*-constraint');

(iii) a set of unsigned unique reflections (with $\lvert F_0\rvert$ known, '*I*-constraint');

(iv) a set of groups of overlapping reflections (with only an intensity sum known for each group, '*G*-constraint').

An illustration of the different constraint types is shown in Fig. 1. Using a simple Fourier transformation to calculate the electron density, one can use only the first set of phased reflections, but has to omit the other three sets. The non-avoidable gaps in the first set often lead to severe disturbances of the density calculated. With a MEM calculation instead, one can use all available information, *i.e.* all four sets, and can reconstruct a strictly positive MEM density, $\rho(\mathbf{r}) \geq 0$, incorporating in this way additional physical pre-knowledge. A MEM density is thus influenced less by the systematic gaps in the set of phased reflections. For our MEM calculations, we used an enhanced version (Burger, 1997) of the program *MEED* (Kumazawa *et al.*, 1993). The original version is available at http://www.mcr.nuap.nagoya-u.ac.jp/mem, while the Tübingen version† is available at http://www.uni-tuebingen.de/uni/pki. A detailed description of the Tübingen version is given in Burger (1998).

1.2.1. *Iterative MEM algorithm*. The electron density ρ is used in a normalized and discretized (pixel) form, and is set equivalent to a probability density, which is calculated by the MEM. The measurement information is introduced through a constraint function C with the 'pseudo-Lagrange parameter' λ. The basic equation is

$$\rho_l = \tau_l \exp\left[-\lambda \partial C/\partial \rho_l\right], \tag{2}$$

used iteratively (Collins, 1982; Sakata & Sato, 1990; Sakata *et al.*, 1990). In one cycle of the iteration, this equation is used for every pixel l of the density: the 'old' density $\rho_l(n)$ of cycle n is used as 'prior' (starting) density τ_l, the constraint function $C(\rho(n), F_{\rm obs}, \sigma(F))$ is calculated using the 'old' density, and a new 'updated' density $\rho_l(n+1)$ results:

$$\rho_l(n+1) = \rho_l(n) \exp\left[-\lambda \partial C(\rho(n), F_{\rm obs}, \sigma(F))/\partial \rho_l\right]. \tag{3}$$

† Changes include *e.g.* modularization of the source code, addition of a program for a corresponding Fourier calculation, improved MEM-constraint divergence and 'lambda' handling, and limitation of the maximum reduction of the constraint function value to 10% maximum, since the original derivation of the MEM algorithm of Collins (1982) is based on small changes in ρ.

The algorithm with its approximations and simplifications is further discussed in Kumazawa *et al.* (1995), Takata & Sakata (1996), and in Burger (1997).

1.2.2. *MEM constraints*.

(*a*) *F-constraints: structure factors* $F = A + iB$ *are completely known*. In the case of known phases [with $\sigma = \sigma(|F|)$, assuming that the structure-factor phases are known from a model calculation and taken to be error free], the constraint function used in the *MEED* program is

$$C_F = (1/N_F) \sum_j^{\text{reflections}} |F_j^c - F_j^o|^2/\sigma_j^2 . \tag{4}$$

(*b*) *I-constraints: known intensities* $|F|^2$. In the case of known intensities [with $\sigma = \sigma(|F|) = \sigma(I)/(2I^{1/2})$], the constraint function is

$$C_I = (1/N_I) \sum_j^{\text{reflections}} ||F_j^c| - |F_j^o||^2/\sigma_j^2. \tag{5}$$

In the *MEED* program, this type of constraint is not specifically implemented. Instead, one uses the *G*-constraint specified below, in the special case of only one reflection per group. Of course, one could also use a constraint function with intensities $|F|^2$ instead of amplitudes $|F|$, but the latter form is better suited for combination with other constraints, as described below.

(*c*) *G-constraints: known intensity sum of a group of reflections, which overlap in a single powder diagram line*. In this case, the constraint function used is (Sakata *et al.*, 1990)

$$C_G = (1/N_G) \sum_j^{\text{groups}} (G_j^c - G_j^o)^2/\sigma_j^2, \tag{6}$$

with $\sigma = \sigma(|G|)$ and the 'mean structure-factor modulus' G_j (m_i multiplicity of reflection i) is

$$G_j = \left(\sum_i^{\text{reflections}} m_i |F_i|^2 \Big/ \sum_i m_i \right)^{1/2}. \tag{7}$$

(*d*) *New A-constraints: 'partly phased' reflections, where* $|F|$, $\cos(\Phi - \Psi_\sigma)$ *and* Ψ_σ *are known*. This constraint type is specially designed for the case of anomalous-scattering information gained from X-ray powder patterns at several wavelengths, as described above.

In this type of experiment, Ψ_σ is known for a specific reflection, and from the measured intensity difference at two wavelengths the quantity A' may be determined completely, but for B' only its modulus may be found:

$$A' \equiv |F| \cos(\Phi - \Psi_\sigma) = A \cos \Psi_\sigma + B \sin \Psi_\sigma$$
$$|B'| \equiv |F||\sin(\Phi - \Psi_\sigma)| = |-A \sin \Psi_\sigma + B \cos \Psi_\sigma|.$$

The constraint function may then be implemented as

$$C_A = (1/N_A) \sum_j^{\text{reflections}} \left[(A_j'^c - A_j'^o)^2/\sigma_{A'j}^2 + (|B_j'^c| - |B_j'^o|)^2/\sigma_{B'j}^2 \right]. \tag{8}$$

In the special case of the resonant atom positioned at the coordinate origin, all Ψ_σ are zero,

$$C_{A0} = (1/N_A) \sum_j^{\text{reflections}} \left[(A_j^c - A_j^o)^2/\sigma_{Aj}^2 + (|B_j^c| - |B_j^o|)^2/\sigma_{Bj}^2 \right]. \tag{9}$$

The equations for the derivatives of the different constraint functions can be found in Appendix *A*.

1.2.3. *Combination of several constraints*. Here a very simple method is used, where the different constraint sums are combined and used together with only one 'Lagrange factor' λ,

$$\rho_l(n+1) = \rho_l(n) \exp\left[-\lambda \left(\frac{\partial C_F}{\partial \rho_l} + \frac{\partial C_I}{\partial \rho_l} + \frac{\partial C_G}{\partial \rho_l} + \frac{\partial C_A}{\partial \rho_l} \right) \right]. \tag{10}$$

In theory, however, one should include each constraint i (to be precise: each measurement and pre-knowledge) with a separate parameter λ_i in the algorithm (Sato, 1992), but in the current *MEED* program the simplified approach described above is used instead. Normalization of the density is not implemented in the form of an additional constraint function, but is performed after each new cycle in the iteration.

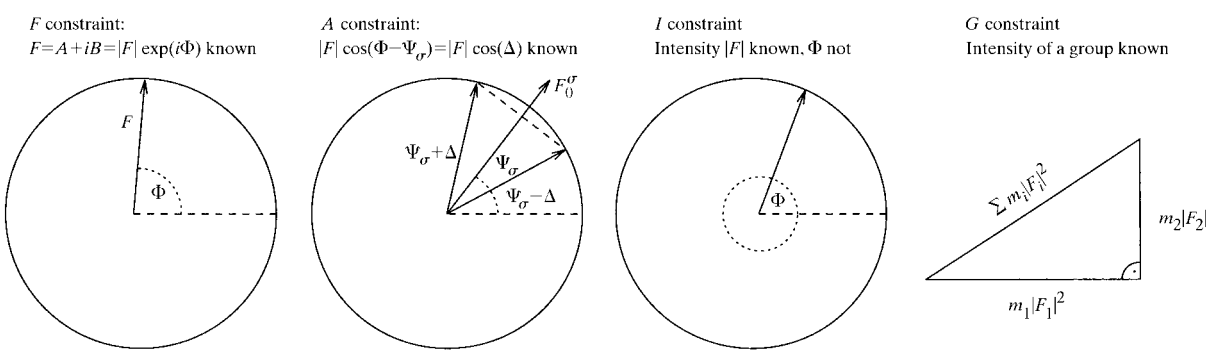

Fig. 1. An illustration of the different constraint types obtained in an anomalous-scattering powder diffraction experiment.

Table 2. *Atom positions in Cu_5Zn_8 clusters*

Name	Atom	Site	Coordinates	Parameters
'Inner tetrahedron' (IT)	Zn1	8(*c*)	(*xxx*)	$x = 0.11$
'Cubo-octahedron' (CO)	Zn2	24(*g*)	(*xxz*)	$x = 0.313$, $z = 0.004$
'Outer tetrahedron' (OT)	Cu1	8(*c*)	(*xxx*)	$x = -0.172$
'Octahedron' (OH)	Cu2	12(*e*)	(*x*00)	$x = 0.356$

1.2.4. *Further remarks*. Usually, a flat starting density is chosen but a non-uniform one could be used in the case of some atom positions already known. One should then be careful not to bias the density too much in the direction of the already known substructure (Papoular & Cox, 1995).

Additional constraints could (and should) also be built into the algorithm to include more knowledge into the calculation, *e.g.* ensure the smoothness of the density maps or a correct nearly Gaussian distribution of the observed around the calculated structure factors [problems of this kind have been reported by Jauch & Palmer (1993); some attempts to overcome this difficulty are discussed by de Vries *et al.* (1994); Yamamoto *et al.* (1996); Iversen *et al.* (1997)]. The constraint functions presented above are in a certain way 'weak constraints', since only sums over all reflections are used [for a mathematical treatment, see Wilkins *et al.* (1983); Sato (1992)].

2. Application to the example Cu_5Zn_8

We use published data of this structure with the measured $|F|$ to simulate an anomalous-scattering experiment using the Cu atoms as resonant scatterers. We proceed gradually from the single crystal to the powder case: along this way much information is lost.

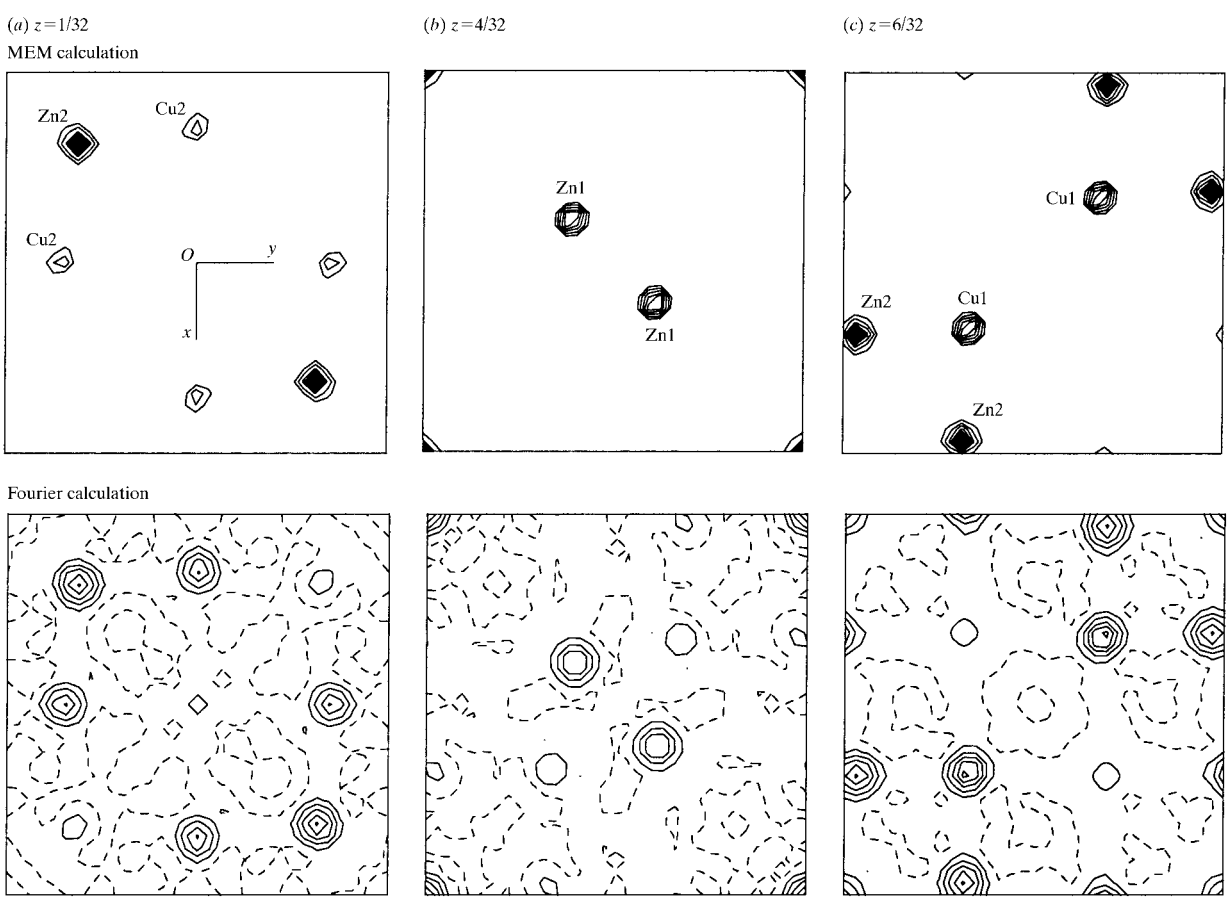

Fig. 2. Three sections through the electron densities of Cu_5Zn_8 calculated with the MEM and the Fourier method (contour line interval: 20 e Å^{-2} for MEM, 10 e Å^{-2} for Fourier maps). The published list of measured structure factors was used, *i.e.* all 70 reflections were used as *F*-constraints with $F = |F| \exp(i\Phi)$ completely known. The Cu2 peaks appear weaker in the MEM-density maps, since the Cu2 position is $z = 0$ and thus not exactly in the plane shown.

Since the structure is noncentrosymmetric, we obtain all types of constraints discussed above. A study of this kind, but with purely synthetic data, can be found in Burger (1997).

2.1. *Cu_5Zn_8 model structure*

The structure of γ-brass Cu_5Zn_8 is cubic, space group $I\bar{4}3m$, with four formula units in the cell and lattice parameter $a = 8.878(4)$ Å. The two kinds of atoms are located on four different positions in clusters of 26 atoms (Brandon *et al.*, 1974). These clusters can be described as nested structures (Table 2).

The first 70 low-order reflections (out of 158) published by Brandon *et al.* (1974) are used (given are measured $|F|$ and calculated Φ; $\sin\theta_{max}/\lambda = 0.574$ Å^{-1}). The reflections 002, 022, 017, 057, 077 are missing in this range. With this data set, a MEM and also a Fourier calculation of the electron density was performed. Since for the MEM calculation the error data $\sigma(|F|)$ are explicitly needed, which are not available from the published data set, we arbitrarily chose an error model of $\sigma(|F|) = 0.01|F|$ for the F- and I-constraints, $\sigma(G) = 0.01G$ for the G-constraints and $\sigma_A = 0.01\max(|A'|,|B'|)$ for the A-constraints. Some characteristic planes in the unit cell are shown in Fig. 2. The MEM density maps show less noise and higher peak-to-background ratio, but also an 'unphysical' sharp peak profile of the stronger peaks, which seems to be inherent in the current algorithm. A remedy would be the use of more high-order reflections or the addition of a constraint for smoothness and maximum peak height. The Fourier density shows a high noise level and regions of negative density, which is mainly a consequence of the missing high-order reflections. The missing reflections 002 *etc.* in the selected angular range would affect the Fourier densities only weakly since the intensities are usually quite low. For a MEM calculation instead, they would be important constraints – if the intensities were zero, the reflections could be used as F-constraints.

2.2. *Simulations with the different constraint types*

Now, with the published structural model we calculate partial structure factors F_0^σ of the copper substructure (Cu1 and Cu2 atoms), assuming that their positions have

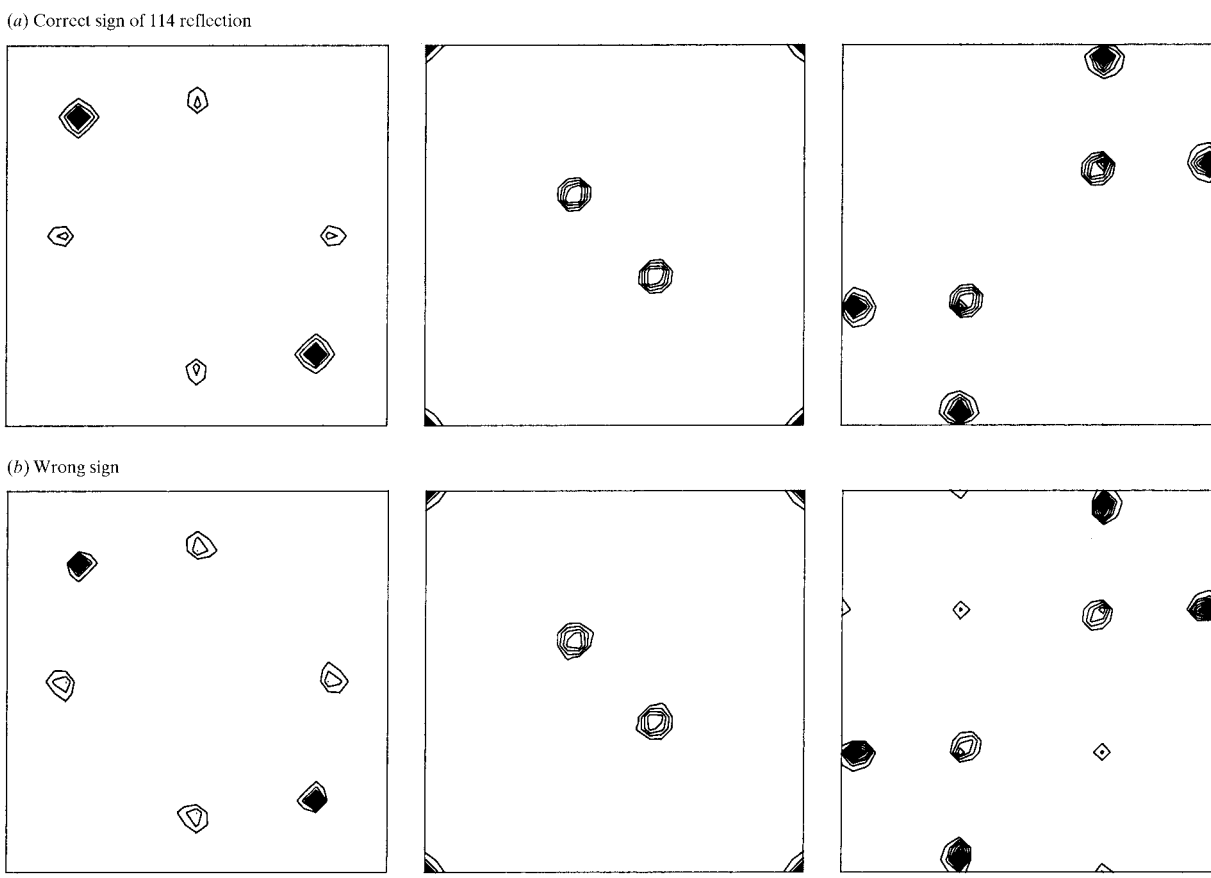

Fig. 3. Result of a MEM calculation simulating the single-crystal case of the new A-constraints (compare with Fig. 2). Only one strong reflection (114) was used as the F-constraint, first with the correct sign (*a*) and in a second calculation with the wrong sign (*b*). The remaining 69 reflections were used as A-constraints, *i.e.* with ambiguity in their phase (1 F-constraint, 69 A-constraints).

been found from difference or partial Patterson maps as described in Burger *et al.* (1997). We have intentionally set the isotropic temperature parameter too large, with $B_{\rm iso} = 1.00$ Å^2 instead of 0.88 and 0.71 Å^2 as published for the two Wyckoff positions of Cu. For this model calculation, we use the program *SIMREF* of our institute (Maichle *et al.*, 1988), which is available in a new version 2.5 from http://www.uni-tuebingen.de/uni/pki.

We then take the published values of the $|F|$ as approximate values of the dispersion-free $|F_0|$, and the published phase angles as the 'true' phase angles Φ, although the authors give a rather high R value $R = \{\sum ||F_{\rm obs}| - |F_{\rm calc}||\}/\{\sum |F_{\rm obs}|\}$ of 6.1% and although the measurement is not completely free of dispersive effects.

With the published values of $|F|$ and Φ and the calculated Ψ_σ(Cu), the values of the A-constraint data $A' \equiv |F| \cos\Delta \equiv |F| \cos(\Phi - \Psi_\sigma)$ and $|B'| \equiv |F| |\sin\Delta|$ were calculated, which would have been measured in an anomalous-scattering experiment using the Cu-edge (at least two measurements: one near but below the edge, with $\lambda > \lambda_{\rm edge}$, and one far-edge). In such an experiment, no Bijvoet differences $I(\mathbf{H}) - I(-\mathbf{H})$ would be obtained, but only dispersive differences $I_{\mathbf{H}}(\lambda_1) - I_{\mathbf{H}}(\lambda_2)$. Calculations were performed on a small workstation (DECstation 5000/120) and took several minutes of calculation time, with a resolution of 32 pixels along the unit-cell edge chosen.

2.2.1. *Single-crystal A-constraint case*. In a first simulation, only the A-constraint information of the 70 reflections was used. The reflection 114 with significant intensity and $|B'|$ was taken as the F-constraint, selecting one of the two possibilities for the sign of $B' = \pm|B'|$. The other 69 reflections were used as A-constraints. The second possibility for B' was then used in a second MEM calculation (Fig. 3). A comparison with the model (Fig. 2) shows very good agreement, with weak 'false peaks' showing up in the case of the wrong sign for B' selected. The calculation with the 'correct' sign converged in 93 cycles of calculation to an R value of 15.9%, while the 'false' sign calculation converged more slowly and to a larger R value, $R = 24.3\%$ after 177 cycles.

It can be seen that the correct density is obtained, although in principle 2^{69} solutions exist, obtained from 69 possible ambiguous choices of the signs of B', which would fit the data given. This surprisingly large number is however significantly reduced, since it is clear that, for reflections with relatively small $|B'|$ values or for very weak reflections, it is usually not important which sign is chosen. That a MEM calculation produces a solution using only one reflection with the correct structure factor indicates the large amount of information contained in the A-constraints, and also the nonlinear character of the algorithm: in an ambiguous situation, a small tendency towards a certain direction is enlarged nonlinearly like a snowball rolling down from the top of a mountain, after being pushed a little out of its unstable position at the top. However, to stay in this picture, there is no guarantee that the snowball always takes the right direction when it rolls faster and faster down the slope. MEM solutions with ambiguous constraints therefore have to be treated cautiously, *e.g.* looking at the solution with "a chemist's eyes". However, this is still a great step forward, since a Fourier calculation with this information is simply not possible.

If the substructure of the r.s. atoms were of higher symmetry than the total structure, it would be possible to obtain two different solutions. This was the case with the structure of $Fe_2Ca_3Ge_3O_{12}$ (Burger *et al.*, 1997) using the absorption edge of the Fe atoms. Also, if for example the r.s. structure was centrosymmetric and the whole crystal not, one could obtain a second solution with simply all signs of the imaginary parts $B' = B$ of $F = A + iB$ inverted, and would get an inverted density, $\rho_{\rm inv}(\mathbf{r}) = \rho_{\rm true}(-\mathbf{r})$. In our case, the general orientation of the solution is given, since one has pre-selected the orientation of the r.s. substructure.†

2.2.2. *The single-crystal A-constraint case using only 'secure' A-constraints*. In a second, more realistic, simulation, we take away all reflections with only a weak contribution of the r.s. from the A-constraint list, using the *ad hoc* criterion $|F_0^\sigma|^2 \leq (1/5)|F|^2$. These reflections are now used with $|F|$ only as (weaker) I-constraints. Thus, 46 A-constraints remain and 23 I-constraints are added. The MEM density calculated (with the correct structure factor of 114) is shown in Fig. 4. It can be seen that the loss of information results in disturbances of the peak shape, while the general features of the density remain the same and all atoms can be located. However, many more cycles were needed to reach a result: the calculations with the correct and the incorrect signs of B' were stopped after 1200 cycles when the calculated R value improved only very slowly. And although the resulting density looks almost the same, the density starting from the 'false' sign converged to $R = 16.1\%$, while the correct sign solution had $R = 18.9\%$ finally, and so a slightly poorer R value.

We also tried to use a weak reflection (112) as the F-constraint, using the correct sign of B' (Fig. 5), but here no acceptable solution was found.

2.2.3. *The powder case with overlapping reflections*. A further significant loss of information occurs, since many reflections coincide in a single powder line owing to the cubic symmetry: in the high-angle region, almost no unique reflections can be found, and up to four members are combined into a group. For each group, only the intensity sum can be measured, resulting in one G-constraint. However, this information is still important, since it reduces the number of possible solutions. Fig. 6 shows the MEM density calculated using the 224

† From Patterson, difference Patterson or partial Patterson densities the correct orientation cannot be extracted, since these densities are centrosymmetric.

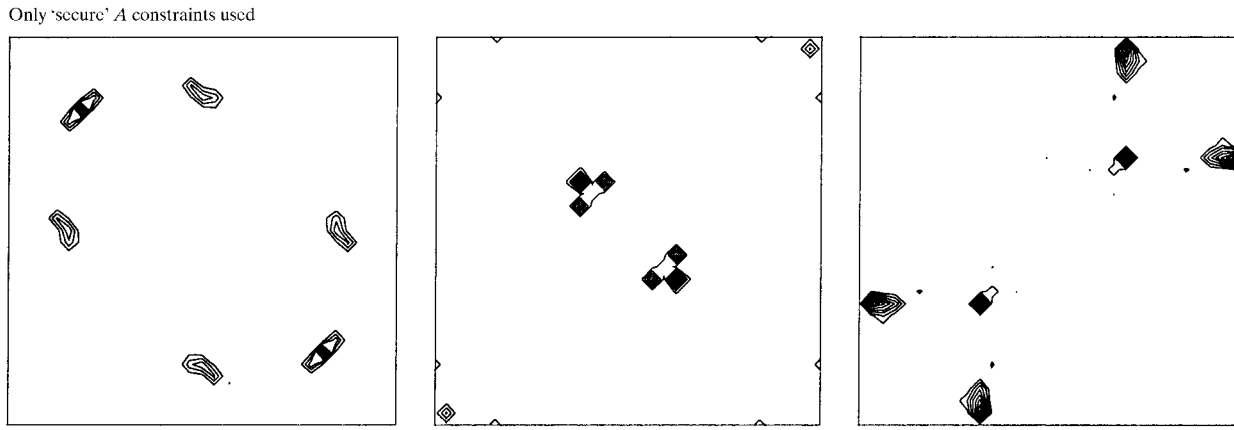

Fig. 4. As Fig. 3(*a*), but taking into account that some unique reflections have only weak contributions of the Cu atoms used as resonant scatterers, so that the *A*-constraint information is not well defined in a real experiment, but only the *I*-constraint information with $|F|$ (1 *F*-constraint, 46 *A*-constraints, and 23 *I*-constraints).

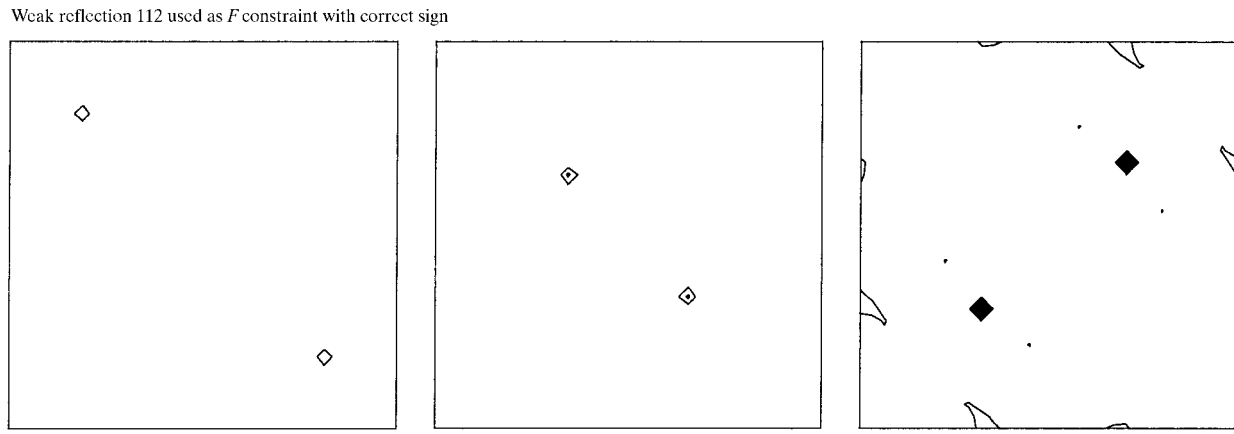

Fig. 5. As Fig. 4, but using a weak reflection (112) as *F*-constraint, with the correct sign selected. This calculation produces no result of sufficient quality.

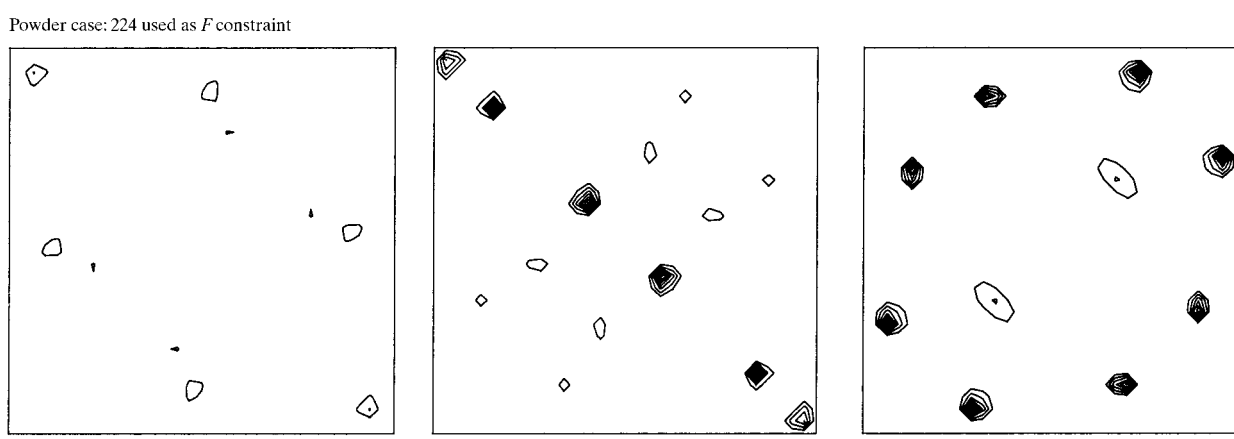

Fig. 6. Simulation of the powder case. Reflections that overlap in the powder diagram were used as *G*-constraints, *i.e.* with their intensity sum information only. The 224 reflection was used as the *F*-constraint with the correct structure factor selected. Thus, 1 *F*-constraint, 15 *A*-constraints, 9 *I*-constraints and 19 *G*-constraints are given. The result is not satisfactory (contour line intervals 10 e Å^{-3} here and in the following figures).

reflection with the correct sign chosen, which is not convincing. It is obvious that we have now reached the limit of the algorithm, since too much information has been lost.

However, it is easy to use another *A*-constraint with its sign arbitrarily chosen, so that now two *F*-constraints are used, and to calculate the MEM solutions for all four combinations of two signs possible. Fig. 7 shows the

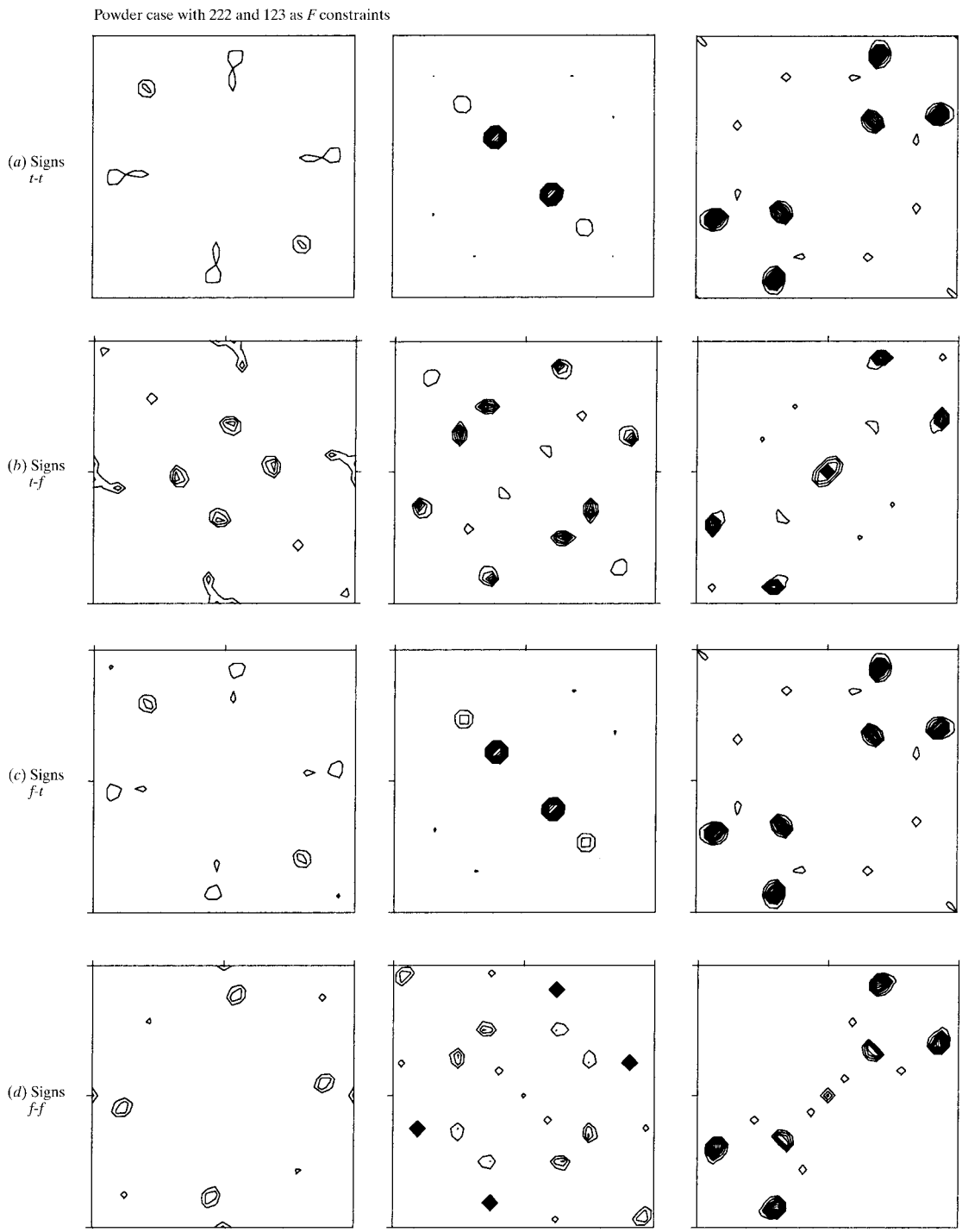

Fig. 7. The powder case is repeated with two *A*-constraint reflections used as *F*-constraints, with four calculations performed for all possible combinations of their signs. The result is much more satisfactory than Fig. 6, and the density quality is sufficient to find the correct solution.

results of these four calculations, using the reflections 222 and 123 as *F*-constraints. The *R* values after 1200 cycles of calculation are 21.1, 27.6, 22.5, 23.6%, respectively, so that the correct sign combination gives the lowest *R* value and the (from inspection) second best density has the second lowest *R* value. However, this feature cannot be guaranteed in all cases. It can be seen that the correct solution can now be found, although the section $z = 1/32$ shows a low peak-density value. In the case of wrong solutions, splitting of peaks and changes in the atomic peak distances may appear.

3. Summary

With the new *A*-constraints, the maximum-entropy method has great advantages over the Fourier calculation of electron densities in the case of anomalous-scattering data sets, since all kinds of information obtained from the experiment can be combined into one MEM calculation:

(i) one set of phased reflections [with $F_0 = |F| \exp(i\Phi)$ known, '*F*-constraint'];

(ii) a set of ambiguous phase informations when only $\cos\Delta$ is known (with $\Delta \equiv \Phi - \Psi_\sigma$ known, '*A*-constraint');

(iii) a set of unsigned unique reflections (with $|F_0|$ known, '*I*-constraint');

(iv) a set of groups of overlapping reflections of a powder diagram (with only the intensity sum known for each group, '*G*-constraint').

In particular, the new *A*-constraints are essential for the use of anomalous-scattering data from powders of noncentrosymmetric crystals that contain only one kind of resonantly scattering atom: in this case, the phase $\Phi(\mathbf{H}) = \Psi_\sigma(\mathbf{H}) \pm \Delta(\mathbf{H})$ of each structure factor can be determined from the experiment only with a remaining ambiguity. A Fourier calculation of the electron density would then be impossible, whereas the MEM calculation uses all available information to calculate the most probable solution compatible with the given data. The MEM program is freely available with Fortran source code, and could be improved further by the introduction of additional constraints and an optimized algorithm. The new quality of the enhanced maximum-entropy method has been clearly demonstrated using the simple noncentrosymmetric example structure of Cu_5Zn_8.

APPENDIX *A*

*A*1. *Derivative* $\partial C_F/\partial\rho_l$ *for the F-constraint*

$F^c = A^c + iB^c$ is the calculated structure factor, F^o the observed structure factor. For the pixel density ρ with total number of (equal-sized) pixels N_{pix} and the total scattering power sum $F(000) \equiv Q$,

$$F^c = \frac{QV_c}{N_{\text{pix}}} \sum_k^{\text{unit cell}} \rho_k \exp(2\pi i \mathbf{H}\cdot\mathbf{r}_k)$$
$$A^c = \frac{QV_c}{N_{\text{pix}}} \sum_k^{\text{unit cell}} \rho_k \cos(2\pi \mathbf{H}\cdot\mathbf{r}_k) \qquad (11)$$
$$B^c = \frac{QV_c}{N_{\text{pix}}} \sum_k^{\text{unit cell}} \rho_k \sin(2\pi \mathbf{H}\cdot\mathbf{r}_k).$$

If N_F constraint values are given, the derivative for pixel l is then

$$\frac{\partial C_F}{\partial\rho_l} = (1/N_F) \sum_j^{\text{reflections}} \frac{1}{\sigma_j^2}\frac{\partial}{\partial\rho_l}\left\{(A_j^c - A_j^o)^2 + (B_j^c - B_j^o)^2\right\}$$
$$= \frac{2QV_c}{N_F N_{\text{pix}}} \sum_j^{\text{reflections}} [(A_j^c - A_j^o)\cos(2\pi\mathbf{H}_j\cdot\mathbf{r}_l) + (B_j^c - B_j^o)\sin(2\pi\mathbf{H}_j\cdot\mathbf{r}_l)]/\sigma_j^2. \qquad (12)$$

*A*2. *Derivative* $\partial C_I/\partial\rho_l$ *for the I-constraint*

This derivative is a special case of the *G*-constraint derivative below, with the reflection treated as a group with one member.

$$\frac{\partial C_I}{\partial\rho_l} = \frac{2QV}{N_I N_{\text{pix}}} \sum_j^{\text{reflections}} \left\{ \frac{|F_j^c| - |F_j^o|}{\sigma_j^2 |F_j^c|} \times \left[A_j^c \cos(2\pi\mathbf{H}_j\cdot\mathbf{r}_l) + B_j^c \sin(2\pi\mathbf{H}_j\cdot\mathbf{r}_l)\right]\right\}. \qquad (13)$$

*A*3. *Derivative* $\partial C_G/\partial\rho_l$ *for the G-constraint*

If N_G constraint values are given, the derivative is

$$\frac{\partial C_G}{\partial\rho_l} = (1/N_G) \sum_j^{\text{groups}} \frac{2}{\sigma_j^2}\left(G_j^c - G_j^o\right)\left(\frac{\partial G_j^c}{\partial\rho_l}\right)$$
$$= \frac{2QV}{N_G N_{\text{pix}}} \sum_j^{\text{groups}} \left\{ \frac{G_j^c - G_j^o}{\sigma_j^2 G_j^c \sum_i m_i} \times \sum_i^{\text{group } j} m_i\left[A_i^c \cos(2\pi\mathbf{H}_i\cdot\mathbf{r}_l) + B_i^c \sin(2\pi\mathbf{H}_i\cdot\mathbf{r}_l)\right]\right\}. \qquad (14)$$

*A*4. *Derivative* $\partial C_A/\partial\rho_l$ *for the new A-constraint*

Using the abbreviations

$$sp \equiv \sin\Psi_\sigma, \qquad cp \equiv \cos\Psi_\sigma$$
$$K_{jl} = \cos(2\pi\mathbf{H}_j\cdot\mathbf{r}_l), \qquad S_{jl} = \sin(2\pi\mathbf{H}_j\cdot\mathbf{r}_l)$$

in an analogous calculation, we obtain

$$\frac{\partial C_A}{\partial \rho_l} = \frac{2QV}{N_A N_{\text{pix}}} \sum_j^{\text{reflections}} \left\{ \frac{A_j'^c - A_j'^o}{\sigma^2_{A'j}} (cpK_{jl} + spS_{jl}) + \frac{|B_j'^c| - |B_j'^o|}{|B_j'^c|\sigma^2_{B'j}} \left[A_j^c [(sp)^2 K_{jl} - spcpS_{jl}] + B_j^c [(cp)^2 S_{jl} - spcpK_{jl}] \right] \right\}. \quad (15)$$

In the special case of all $\Psi_\sigma = 0$, *i.e.* the r.s. are located at the unit-cell origin, this is equal to

$$\frac{\partial C_{A0}}{\partial \rho_l} = \frac{2QV}{N_A N_{\text{pix}}} \sum_j^{\text{reflections}} \left[\frac{(A_j^c - A_j^o)\cos(2\pi \mathbf{H}_j \cdot \mathbf{r}_l)}{\sigma^2_{Aj}} + \frac{(|B_j^c| - |B_j^o|)\,\text{sign}(B_j^c)\sin(2\pi \mathbf{H}_j \cdot \mathbf{r}_l)}{\sigma^2_{Bj}} \right]. \quad (16)$$

Note: in the program *MEED*, the constant $2QV/N_{\text{pix}}$ is omitted, thus including it in the λ (lambda) parameter.

We acknowledge financial support by the German ministry for research (BMBF, project No. 05 647 VTA).

References

Bourenkov, G. P., Popov, A. N. & Bartunik, H. D. (1996). *Acta Cryst.* A**52**, 797–811.

Brandon, J. K., Brizard, R. Y., Chieh, P. C., McMillan, R. K. & Pearson, W. B. (1974). *Acta Cryst.* B**30**, 1412–1417.

Bricogne, G. & Gilmore, C. J. (1990). *Acta Cryst.* A**46**, 284–297.

Burger, K. (1997). PhD thesis, Universität Tübingen. Aachen: Shaker.

Burger, K. (1998). *Powder Diffr.* **13**, 117–120.

Burger, K., Cox, D., Papoular, R. & Prandl, W. (1998). *J. Appl. Cryst.* **31**, 789–797.

Burger, K., Prandl, W. & Doyle, S. (1997). *Z. Kristallogr.* **212**, 493–505.

Collins, D. (1982). *Nature (London)*, **298**, 49–51.

Gilmore, C. J. (1996). *Acta Cryst.* A**52**, 561–589.

Haibach, T. & Steurer, W. (1996). *Acta Cryst.* A**52**, 277–286.

Hendrickson, W. (1991). *Science*, **254**, 51–58.

Iversen, B. B., Jensen, J. L. & Danielsen, J. (1997). *Acta Cryst.* A**53**, 376–387.

Jauch, W. & Palmer, A. (1993). *Acta Cryst.* A**49**, 590–591.

Kumazawa, S., Kubota, Y., Takata, M., Sakata, M. & Ishibashi, Y. (1993). *J. Appl. Cryst.* **26**, 453–457.

Kumazawa, S., Takata, M. & Sakata, M. (1995). *Acta Cryst.* A**51**, 47–53.

Limper, W., Prandl, W. & Wroblewski, T. (1991). *Mater. Sci. Forum*, **79–82**, 221–226.

Maichle, J. K., Ihringer, J. & Prandl, W. (1988). *J. Appl. Cryst.* **21**, 22–27.

Papoular, R. J. & Cox, D. (1995). *Europhys. Lett.* **32**, 337–342.

Papoular, R. J., Prandl, W. & Schiebel, P. (1992). In *Maximum Entropy and Bayesian Methods.* Dordrecht: Kluwer.

Papoular, R. J., Zheludev, A., Ressouche, E. & Schweizer, J. (1995). *Acta Cryst.* A**51**, 295–300.

Prandl, W. (1990). *Acta Cryst.* A**46**, 988–992.

Prandl, W. (1994). *Acta Cryst.* A**50**, 52–55.

Sakata, M., Mori, R., Kumazawa, S., Takata, M. & Toraya, H. (1990). *J. Appl. Cryst.* **23**, 526–534.

Sakata, M. & Sato, M. (1990). *Acta Cryst.* A**46**, 263–270.

Sato, M. (1992). *Acta Cryst.* A**48**, 842–850.

Schleger, P., Puig-Molina, A., Ressouche, E., Rutty, O. & Schweizer, J. (1997). *Acta Cryst.* A**53**, 426–435.

Sivia, D. S. & David, W. I. F. (1994). *Acta Cryst.* A**50**, 703–714.

Takata, M. & Sakata, M. (1996). *Acta Cryst.* A**52**, 287–290.

Takata, M., Sakata, M., Kumazawa, S., Larsen, F. K. & Iversen, B. B. (1994). *Acta Cryst.* A**50**, 330–337.

Vries, R. Y. de, Briels, W. J. & Feil, D. (1994). *Acta Cryst.* A**50**, 383–391.

Wilkins, S. W., Varghese, J. M. & Lehmann, M. S. (1983). *Acta Cryst.* A**39**, 47–60.

Yamamoto, K., Takahashi, Y., Ohshima, K., Okamura, F. P. & Yukino, K. (1996). *Acta Cryst.* A**52**, 606–613.